Dehydrogenation of Formic Acid Promoted by a Trihydride-Hydroxo-Osmium (IV) Complex: Kinetics and Mechanism

Miguel A. Esteruelas, Cristina García-Yebra, Jaime Martín, and Enrique Oñate*

Departamento de Química Inorgánica, Instituto de Síntesis Química y Catálisis Homogénea (ISQCH), Centro de Innovación en Química Avanzada (ORFEO-CINQA), Universidad de Zaragoza-CSIC, 50009 Zaragoza, Spain

ABSTRACT

The preparation of the hydroxo-osmium(IV) complex $OsH_3(OH)\{xant(P^iPr_2)_2\}$ ($xant(P^iPr_2)_2$ = 9,9-dimethyl-4,5-bis(diisopropylphosphino)xanthene) and its catalytic efficiency for the dehydrogenation of formic acid to H_2 and CO_2 are reported. The mechanism of the dehydrogenation has been unambiguously stablished by combining the kinetic analysis of the catalysis, the isolation of the intermediates and the kinetic analysis of their decomposition, and DFT calculations on the rate-determining step. Under catalytic conditions the trihydride-hydroxo complex reacts with formic acid to afford $OsH_3\{\kappa^1\text{-}O\text{-}(HCO_2)\}\{xant(P^iPr_2)_2\}$, which isomerizes into $OsH_3\{\kappa^1\text{-}H\text{-}(HCO_2)\}\{xant(P^iPr_2)_2\}$ by means of the slippage of the metal center through a formate O-C-H path. The κ^1-H-formate intermediate releases CO_2 to give the previously reported

tetrahydride $OsH_4\{xant(P^iPr_2)_2\}$, which undergoes protonation with formic acid. The resulting OsH_5-cation exists as an equilibrium mixture of the tautomers trihydride-compressed dihydride $[OsH_3(H\cdots H)\{xant(P^iPr_2)_2\}]^+$ and hydride-compressed dihydride-dihydrogen $[OsH(H\cdots H)(\eta^2\text{-}H_2)\{xant(P^iPr_2)_2\}]^+$. The dissociation of H_2 from the latter leads to $[OsH_3\{xant(P^iPr_2)_2\}]^+$, which coordinates HCO_2^- to regenerate the trihydride-(κ^1-O-formate) complex and to close the cycle. The release of CO_2 from the κ^1-H-formate intermediate is the rate-determining step of the catalysis.

INTRODUCTION

Hydrogen gas is a promising energy carrier as clean alternative to conventional fossil fuels. It can be produced from any primary energy source, has an energy content per mass that is about three times that of the carbon-based fuels, can be used by direct introduction into either an internal combustion engine or to a fuel cell, and its oxidation with O_2 gives water.[1] However, its energy content per volume is very low at standard temperature and pressure. To overcome this difficulty, several methods are being investigated.[2]

The concept of chemical storage is an attractive strategy; in particular the use of organic liquids since they can be transported through the liquid-fuel infrastructures. In these compounds, hydrogen does not exist in its molecular form but is covalently bound. At the time and place of energy demand, H_2 is released via dehydrogenation. The hydrogen carrying liquid itself is not consumed but is reloaded and used in further cycles.[3] Formic acid is a reputed family member of liquid organic hydrogen carriers. It is stable under ambient conditions, produced in large-scale, and biodegradable. Furthermore, it has low flammability and toxicity, its gravimetric and volumetric H_2 capacity of 4.4 wt. % and 53.4 g/L are reasonable,[4] and its recyclability by means

CO_2 hydrogenation undergoes a constant improvement,[5] reaching complex RuHCl(CO)(PNP) (PNP = 2,6-bis(di-*ter*-buthylphosphinomethyl)pyridine) a TOF of 1100000 h^{-1} for the reduction to formates in 2014.[5a]

Both homogeneous and heterogeneous transition metal systems have proven to have the ability of promoting the formic acid (FA) dehydrogenation to H_2 and CO_2.[6] The majority of the homogeneous catalysts are complexes of Fe,[7] Ru,[8] and Ir.[9] In addition, a few precursors of Mo,[10] Rh,[11] Ni,[12] Cu,[13] and Al[14] have been also reported. Further research needs to be focused on the mechanism of the whole catalytic process. Most of them are only postulated and experimental support is necessary. The catalysis has two stages, CO_2 formation and H_2 formation. The rate-limiting step can be any of them. The main divergences are found in the former, which may happen by hydride abstraction, β-hydride elimination, or by an outer-sphere mechanism.[15] Although the latter is currently questioned.[16]

The use of Os in homogeneous catalysis has received significantly less attention than the use of its group congeners Fe and Ru. With the exception of Sharpless dihydroxylation and processes akin,[17] it has been centered in some particular reactions of organic synthesis.[18] However, in the last years, it is being revealed as a promising alternative for processes related to the hydrogen economy.[19] Of special relevance are its polyhydride derivatives,[20] which have shown to have the ability of carrying out the dehydrogenation of amineboranes[21] and liquid organic hydrogen carriers such as alcohols and cyclic amines.[22] Other ligand with good performance is the hydroxo group. For instance, complex [Os(OH)(η^6-*p*-cymene)IPr]OTf (IPr = 1,3-bis(2,6-diisopropylphenyl)imidazolylidene; OTf = CF_3SO_3) has shown great efficiency in the hydrogen transfer from 2-propanol to aldehydes,[23] the α-alkylation of arylacetonitriles and methyl ketones,[24] and the hydration of nitriles to amides.[25]

Hydroxo complexes of the platinum group metals are very scarce and their chemistry is underdeveloped.[26] Hydride-hydroxo derivatives are particularly challenging since formally result from the oxidative addition of water, which is generally disfavored from a thermodynamic point of view and thus the limited known examples display reversibility.[27] Compounds of Os of this class are Os(II)-species[28] and, although the oxidation state +4 is usual for this element when bears small size ligands, the hydride-hydroxo-Os(IV) complexes are unknown until now.

Pincer ligands show a marked ability to stabilize uncommon complexes due to the disposition of their donor atoms.[29] Ether-diphosphines have particular interest due to their flexibility, which grant the ability of changing between κ^3-*mer*-, κ^3-*fac*, and κ^2 coordination modes. This allows them to adapt to the requirements of the participating intermediates of the catalytic cycles.[30] In the search for efficient catalysts for processes related to hydrogen economy and also for reactions of interest in organic synthesis, some years ago we initiated a research program on POP complexes of groups 8[19c,30c,30i,31] and 9,[30h,32] which has yielded us to discover notable catalysts for dehydrogenation of ammonia borane,[30h] monoalcoholysis of disilanes,[32b] synthesis of imines from alcohols and amines with liberation of H_2,[19c] hydrogen transfer from 2-propanol to ketones, α-alkylation of phenylacetonitrile and acetophenone with alcohols,[31b] regio- and stereoseletive head-to-head (*Z*)-dimerization of terminal alkynes,[30c,31b] borylation of arenes,[32c] and decyanative borylation of arylnitriles.[32d] Now, we have discovered that the ether-diphosphine 9,9-dimethyl-4,5-bis(diisopropylphosphino)xanthene (xant(P^iPr_2)$_2$) stabilizes a hydride-hydroxo-Os(IV) complex, which efficiently promotes the FA dehydrogenation. This paper reports the preparation and characterization of this novel catalyst precursor, its activity in the dehydrogenation process, and the kinetics and mechanism of the same one.

RESULTS AND DISCUSSION

Preparation and Characterization of the Catalyst Precursor. The known hydroxo compounds of osmium include the nitrido complexes $Os(N)Tp(OH)_2$ (Tp = hydridotris(1-pyrazolyl)borate),[33] $[Os(N)(CH_2SiMe_3)(OH)]^-$, and $[Os(N)(CH_2SiMe_3)(OH)_2]^-$,[34] the previously mentioned cation $[Os(OH)(\eta^6\text{-}p\text{-cymene})IPr]^+$,[23] the hydride-hydroxo derivatives $OsH(OH)(PMe_3)_4$,[28a] $OsH(OH)(CO)(PR_3)_2$ (PR_3 = P^iPr_3,[28b] P^tBu_2Me[28c]), $OsH(OH)(NH_2CMe_2CMe_2NH_2)(PPh_3)_2$,[28d] and $[OsH(OH)(C{\equiv}CPh)(IPr)(P^iPr_3)]OTf$,[28e] and a few dimers.[35] They were prepared by one of these methods: hydrolysis of Os-C[28a,28c] or Os-N[28d] bonds and replacement of chloride by hydroxo.[23,28a,28c,34] The first method is not suitable in our case by the lack of an appropriate starting compound. So, we tried the substitution of chloride by hydroxo employing the previously reported[30c] trihydride $OsH_3Cl\{xant(P^iPr_2)_2\}$ (**1**) as a precursor. However, all attempts were unsuccessful, reaching a partial substitution in the best of cases. Then, we decided to replace the chloride ligand of **1** by a better leaving group as trifluoromethanesulfonate (Scheme 1).

Scheme 1. Preparation of complex 3

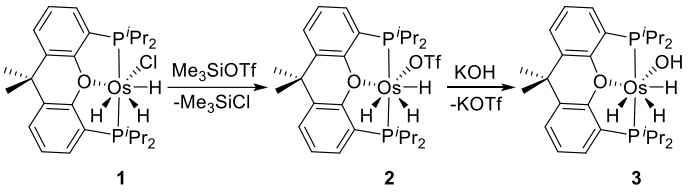

Treatment of a toluene solution of **1** with 2.0 equiv of Me_3SiOTf, at room temperature, for 10 min affords the synthetic intermediate $OsH_3(OTf)\{xant(P^iPr_2)_2\}$ (**2**), which was isolated as a yellow solid in 90 % yield. The substitution reaction is supported by the ^{19}F NMR spectrum, in toluene-d_8, which shows a singlet at -77.7 ppm due to the coordinated OTf^- anion. Like observed for its chloride precursor, the ^1H NMR spectrum of **2** in toluende-d_8 shows a resonance at -13.82 ppm for the inequivalent hydride ligands, which indicates the operation of two thermally

activated site exchange processes within the OsH_3 unit. Between 233 and 223 K, decoalescence occurs and two signals at -12.12 and -17.02 ppm in a 2:1 intensity ratio are observed. Although at lower temperatures than 223 K the resonance at -12.12 ppm displays broad, the expected second decoalescence is not reached even at 183 K. According to the trihydride character of the compound, 400 MHz T_1(min) values of 89 ± 4 and 69 ± 3 ms were found at 223 K for the hydride resonances. The $^{31}P\{^1H\}$ NMR spectrum shows a singlet at 54.6 ppm between 298 and 183 K.

Trifluromethanesulfonate is easily displaced by a hydroxo group, in contrast to the chloride ligand of **1**. Dropwise addition of a water KOH solution to an acetone solution of **2** at room temperature leads to the hydroxo $OsH_3(OH)\{xant(P^iPr_2)_2\}$ (**3**), which was isolated as a yellow solid in 92 % yield. The presence of the hydroxo ligand in this novel osmium(IV) species is supported by the IR and ^1H NMR spectrum. The IR contains the characteristic ν(OH) band at 3672 cm^{-1}, whereas the ^1H NMR spectrum in toluene-d_8 shows a broad resonance at 2.87 ppm corresponding to the OH-hydrogen atom. Like the ^1H NMR spectrum of **2**, the spectrum contains a signal (δ_{1H}, -12.25) for the hydrides, indicating that are also involved in two thermally activated site exchange processes. At about 273 K, a first decoalescence occurs to give two resonances at -12.46 and -13.08 ppm in a 2:1 intensity ratio. Between 203 and 193 K, the lower field signal splits into an AB system. The J_{AB} coupling constant decreases from 151.9 to 146.8 Hz as the temperature does from 193 to 173 K. These unusually high value for two hydrides disposed *cis* and their dependence with the temperature can be rationalized in terms of quantum-mechanical exchange coupling between the involved hydrides.[20] The $^{31}P\{^1H\}$ NMR spectrum shows a singlet at 49.9 ppm.

FA Dehydrogenation Promoted by 3: Kinetic Study. Trihydride-hydroxo complex **3** promotes the FA dehydrogenation to H_2 and CO_2.[36] It works well with diluted solutions and also dehydrogenates neat formic acid, but rapidly decomposes under the latter conditions. The reactions were performed in toluene, under atmospheric pressure, between 298 to 318 K. The partial volume of hydrogen formed (V_{H_2}) was determined from the total volume (V_T) of gas generated according to eq 1, where $V_{m(H_2)}$ and $V_{m(CO_2)}$ are the partial molar volumes of H_2 and CO_2, respectively. The total volume was measured by displacing vaseline oil from a gas burette.

$$V_{H_2} = [V_T/(V_{m(H_2)} + V_{m(CO_2)})]V_{m(H_2)} \qquad (1)$$

The kinetics of the catalysis was studied to gain insight into the process. Initial rates (Table 1) were determined from the gas evolution experiments (Figure 1) by using eq 2, where P is the atmospheric pressure (atm), *R* is the molar gas constant, T is the temperature (K) and V_{sol} is the total volume of the reaction solution.

$$d[H_2]/dt = (dV_{H_2}/dt)P/RTV_{sol} \qquad (2)$$

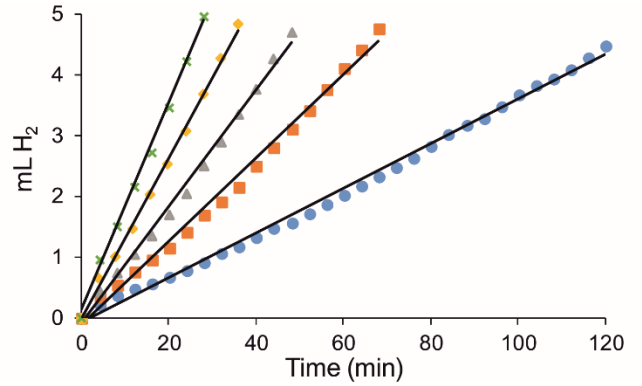

Figure 1. V_{H_2} Generated from the catalytic dehydrogenation of H_2CO_2 (0.53 M) promoted by **3** in toluene at 298 K. 10^2[**3**]: 0.61 M (blue circle), 1.23 (orange square), 1.86 (grey triangle), 2.48 (yellow diamond), 3.06 (green cross).

Table 1. Kinetic data for the dehydrogenation of formic acid promoted by 3[a]

T (K)	10^2[**3**] (M)	$[H_2CO_2]_0$ (M)	10^2d$[H_2]$/dt [b] (M·min^{-1})	k (min^{-1})
298	0.61	0.53	0.057	0.094
298	1.23	0.53	0.123	0.100
298	1.86	0.53	0.155	0.083
298	2.48	0.53	0.228	0.092
298	3.06	0.53	0.278	0.091
298	1.23	0.42	0.118	0.096
298	1.23	0.64	0.124	0.101
298	1.23	0.74	0.128	0.104
298	1.23	0.95	0.128	0.104
303	1.24	0.53	0.216	0.174
308	1.24	0.53	0.370	0.298
313	1.23	0.53	0.503	0.409
318	1.23	0.53	0.914	0.743

[a] Reactions were quantitative yielding TON between 17 and 87. [b] Calculated at 20% conversion.

A rate law for the dehydrogenation of formic acid promoted by **3** is

$$\mathrm{d[H_2]/dt} = k[\mathrm{H_2CO_2}]_0^{\mathrm{a}}[\mathbf{3}]^{\mathrm{b}} \qquad (3)$$

The rate dependence on formic acid concentration was determined at 298 K, for a constant concentration of **3** of $1.23 \cdot 10^{-2}$ M, by measuring initial rates with variable initial concentrations of formic acid ($[H_2CO_2]_0$ in Table 1) from 0.42 to 0.95 M. Under these conditions, the rate is independent of $[H_2CO_2]_0$ within the experimental error (Figure 2), in agreement with a = 0 in eq 3. The rate dependence on the catalyst precursor **3** was also determined at 298 K, for a fixed

initial concentration of formic acid of 0.53 M, by varying the concentration of **3** from $0.61 \cdot 10^{-2}$ to $3.06 \cdot 10^{-2}$ M. Now, the plot of $\ln(d[H_2]/dt)$ versus ln[**3**] affords a straight line of slope 0.96 ± 0.17 (Figure 3), according to a first order in osmium concentration (b = 1 in eq 3). Therefore, the rate law is:

$$d[H_2]/dt = k[\mathbf{3}] \qquad (4)$$

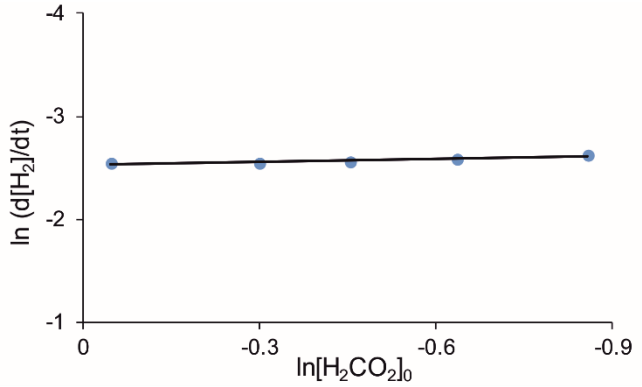

Figure 2. Plot of $\ln(d[H_2]/dt)$ vs $\ln[H_2CO_2]_0$ in toluene at 298 K, for a constant [**3**] of $1.23 \cdot 10^{-2}$ M.

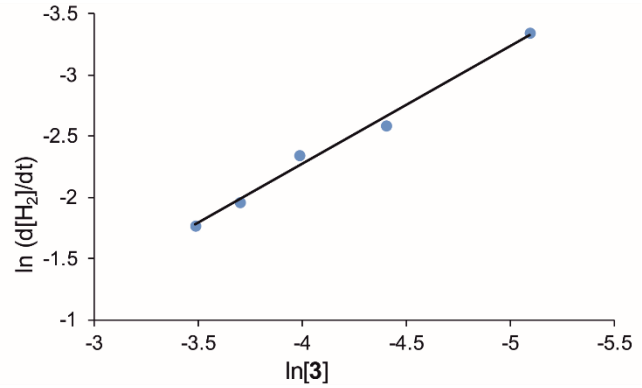

Figure 3. Plot of $\ln(d[H_2]/dt)$ vs ln[**3**] in toluene at 298 K, for a constant $[H_2CO_2]_0$ of 0.53 M.

A plot of $d[H_2]/dt$ versus [**3**] (Figure 4) provides a value of $9.0 \pm 1.0 \cdot 10^{-2}$ min^{-1} for *k* at 298 K. The activation parameters obtained from the Eyring analysis (Figure 5) are $\Delta H^{\ddagger}$ = 18 ± 3 kcal·mol^{-1} and $\Delta S^{\ddagger}$ = -3 ± 8 cal·mol^{-1}K^{-1}, which yield a $\Delta G^{\ddagger}$ value of 18 ± 5 kcal·mol^{-1} at 298 K

in agreement with the values reported for the dehydrogenation of formic acid catalyzed by other homogeneous systems (17 – 26 kcal·mol^{-1}).[5a, 7d, 9f, 37]

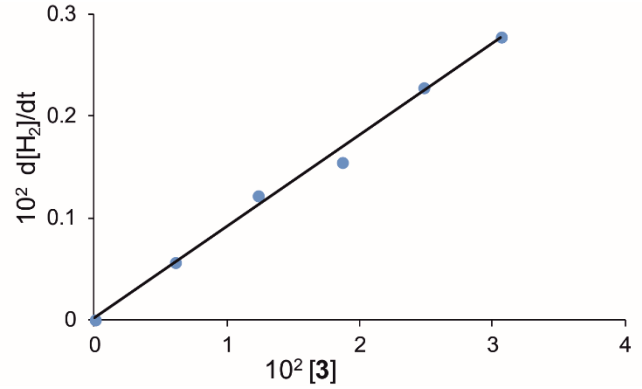

Figure 4. Plot of d[H_2]/dt vs [**3**] using 0.53 M of H_2CO_2 in toluene at 298 K.

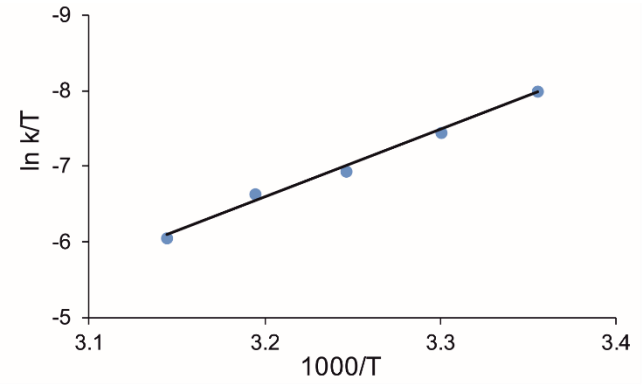

Figure 5. Eyring plot for the dehydrogenation of formic acid (0.53 M) promoted by **3** ($1.23 \cdot 10^{-2}$ M) in toluene.

Stoichometric Reactions. In order to have access to the key intermediates of the catalysis, we studied the stoichiometric reaction of **3** with formic acid in addition to the stages of CO_2 and H_2 formation.

The addition of 1.0 equiv of formic acid to a toluene-d_8 solution of **3** contained in a NMR tube quantitatively and instantly leads to the formate derivative $OsH_3\{\kappa^1\text{-O-}(HCO_2)\}\{xant(P^iPr_2)_2\}$

(**4**), as a consequence of the protonation of the hydroxo ligand of **3** and the subsequent displacement of the generated H_2O by a formate anion (Scheme 2).

Scheme 2. Reaction of 3 with H_2CO_2

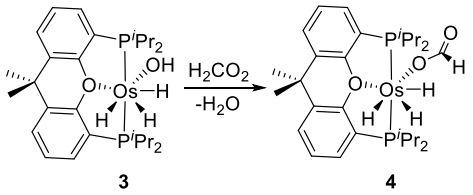

The presence of a formate group in the osmium coordination sphere is supported by $^{13}C\{^1H\}$ and ^1H NMR spectra of the new species at 253 K. The $^{13}C\{^1H\}$ NMR spectrum shows at 167.8 ppm a singlet due to the HCO_2-carbon atom, whereas the ^1H NMR spectrum contains a singlet at 8.91 ppm corresponding to the HCO_2-hydrogen atom. Like in **2** and **3**, the hydrides of **4** experience position exchange thermally activated. Thus, they display a broad signal at -12.55 ppm. At about 213 K, a first decoalescence occurs to afford two signals at -12.00 and -13.32 ppm. At 193 K, the expected second decoalescence can be intuited from the very broad form of the resonance at -11.93 ppm. In the $^{31}P\{^1H\}$ NMR spectrum, the diphosphine gives rise to a singlet at 51.2 ppm. These spectroscopic features are consistent with the stereochemistry proposed for **4** in Scheme 2, which was confirmed by the X-ray diffraction analysis of a single crystal obtained from the toluene-d_8 solution (Figure 6). The Os{xant(P^{i}Pr$_2$)$_2$} skeleton is T-shaped with the metal center situated in the common vertex and P1-Os-P2, P1-Os-O3, and P2-Os-O3 angles of 159.84(7)º, 83.08(12)º, and 82.63(12)º, respectively. The geometry around the osmium atom can be described as a distorted pentagonal bipyramid with axial P^{i}Pr$_2$ groups and the oxygen atoms of the diphosphine and formate in the perpendicular plane, mutually *cisoid* disposed, along with the hydrides.

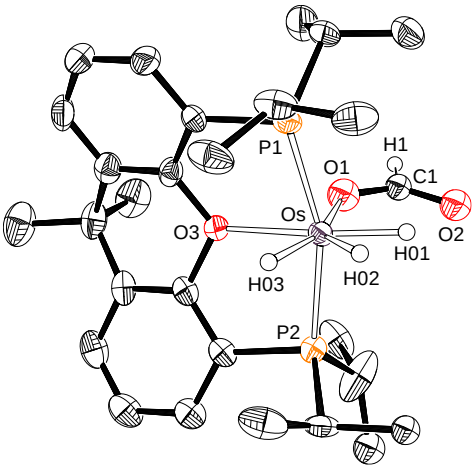

Figure 6. Molecular drawing of **4** with 50% probability ellipsoids. Hydrogen atoms (except hydrides and H1) are omitted. Selected distances (Å) and angles (deg): Os-O3 = 2.231(4), Os-O1 = 2.137(6), Os-P1 = 2.2915(19), Os-P2 = 2.2848 (18); P1-Os-P2 = 159.84(7), P1-Os-O3 = 83.08(12), P2-Os-O3 = 82.63(12), O1-Os-O3 = 76.1(3)

Complex **4** is unstable and releases CO_2 to afford $OsH_4\{xant(P^iPr_2)_2\}$ (**5**), according to Scheme 3. The transformation was monitored by $^{31}P\{^1H\}$ NMR spectroscopy as a function of time between 303 and 323 K. Figure 7 shows the transformation at 323 K. The decrease of **4** is an exponential function of time, in agreement with a first-order process, which fits to the expression

$$\ln([\mathbf{4}]/[\mathbf{4}]_0) = k_{st}t \qquad (5)$$

where $[\mathbf{4}]_0$ is the initial concentration of **4** and [**4**] is the concentration at time t. The values for the stoichiometric rate constant k_{st} are collected in Table 2. The activation parameters calculated by means of the Eyring analysis (Figure 8) are $\Delta H^{\ddagger} = 20 \pm 3$ kcal·mol^{-1} and $\Delta S^{\ddagger} = 0 \pm 8$ cal·mol^{-1}K^{-1}. They affords a $\Delta G^{\ddagger}$ value of 20 ± 5 kcal·mol^{-1} at 298 K, which compares well with that obtained for the catalytic process.

Scheme 3. Decarboxylation of complex 4

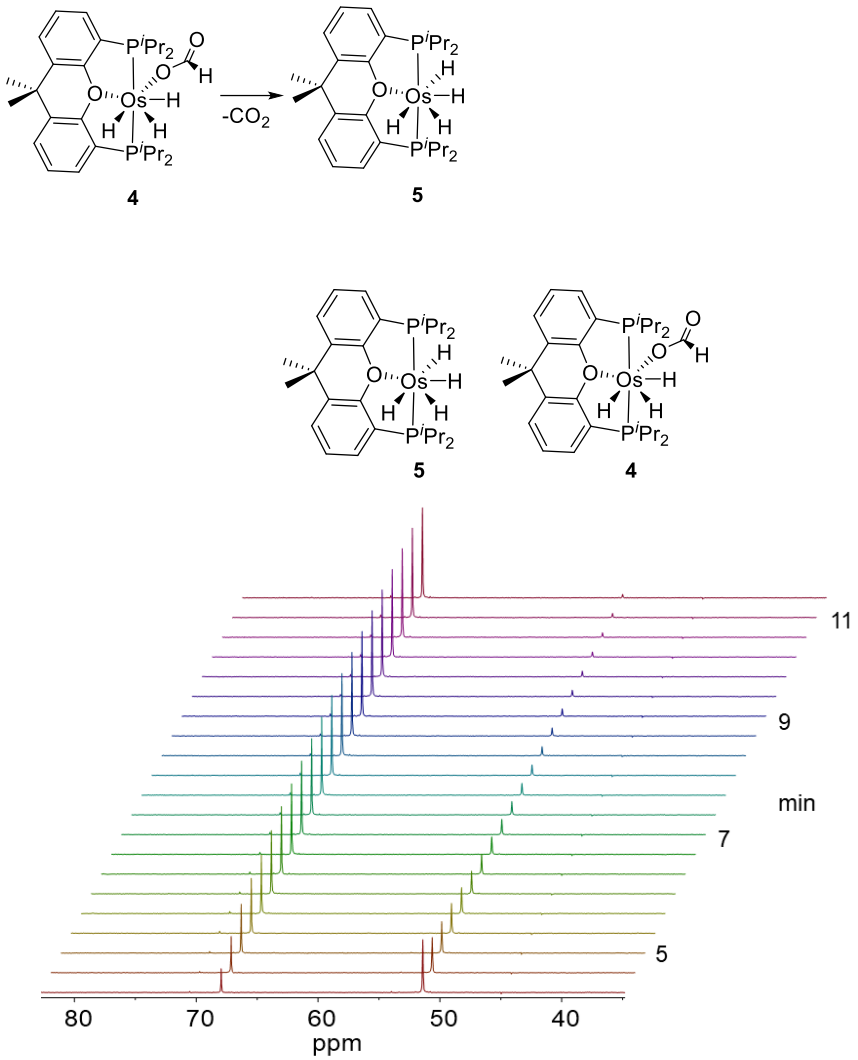

Figure 7. $^{31}P\{^1H\}$ spectra (161.98 MHz, in toluene-d_8) for the transformation of **4** into **5** at 323 K.

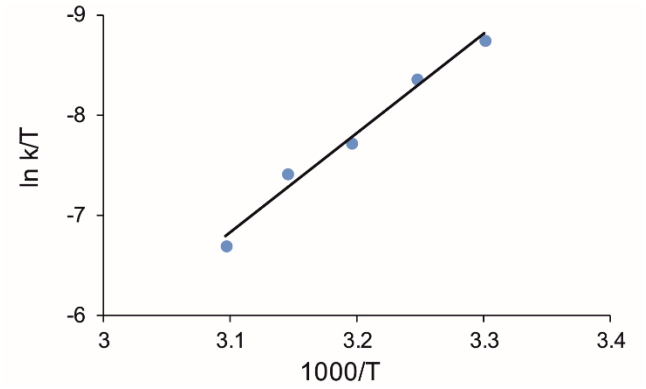

Figure 8. Eyring plot for the decarboxylation of **4** ($6.4 \cdot 10^{-2}$ M) in toluene-d_8.

Table 2. **Rate Constants k_{st} for the Decarboxylation of 4**

T (K)	k_{st} (min^{-1})
303	0.048
308	0.072
313	0.138
318	0.192
323	0.396

Tetrahydride complex **5** reacts with FA to form molecular hydrogen and to regenerate the formate derivative **4** (Scheme 4). At 243 K, the addition of 1.0 equiv of formic acid to a toluene-d_8 solution of **5** rapidly gives **4** and H_2 in quantitative yield. According to previous studies, the reaction initially implies the protonation of **4** to afford an OsH_5-cation **A**. DFT-Calculations revealed that this cation has two tautomers with similar energies: the trihydride compressed dihydride **Aa** and the hydride-compressed dihydride-dihydrogen **Ab**.[30c] The dissociation of the coordinated H_2 ligand from the latter and the coordination of the formate anion to the resulting unsaturated species **B** should lead to **4**.

Scheme 4. Reaction of 5 with H_2CO_2

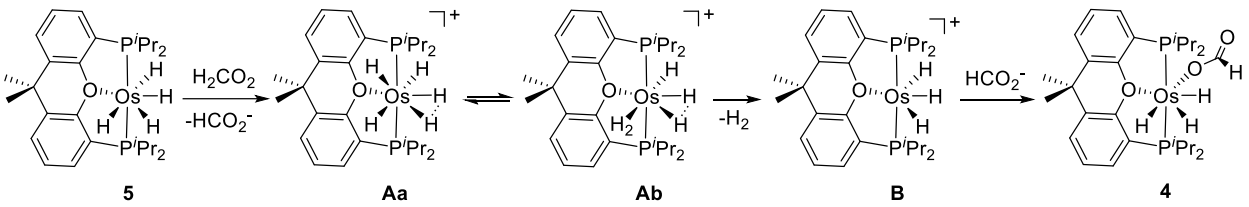

The reactions summarized in Schemes 2-4, fully characterize the catalysis. The trihydride-hydroxo complex **3** is the precursor of the catalyst and, under catalytic conditions, is quantitatively transformed into the true catalyst, the formate derivative **4** (Scheme 2), which releases CO_2 to form the tetrahydride **5** (Scheme 3). The latter reacts with FA to produce molecular hydrogen and regenerate **4** in a three step process: protonation, H_2 dissociation, and formate coordination (Scheme 4). Because the catalytic FA dehydrogenation promoted by **3** has the same activation parameters as the stoichiometric release of CO_2 from **4**, the CO_2 formation is the rate determining step of the catalysis, while the molecular hydrogen formation is fast.

Mechanism of the CO_2 Formation Stage. As previously mentioned the CO_2 formation stage can occur through three different pathways: outer-sphere, *β*-hydride elimination, and hydride abstraction. An outer-sphere pathway must be excluded in this case because the system does not bear any function which could allow such catalysis class. *β*-Hydride elimination reactions have been proposed in cycles initiated by half-sandwich iridium(III) derivatives;[9f, 9i,] ruthenium complexes bearing pincer PNP ligands;[8e] iron species stabilized by PPP groups;[7c] and catalysts generated in situ from $Fe_3(CO)_{12}$, 2,2':6'2''-terpyridine or 1,10-phenanthroline, and triphenylphosphine working under visible light irradiation,[7b] among others. A distinctive fact of this mechanism is that the *β*-hydride elimination step occurs on unsaturated species. Hydride abstraction has been mainly proposed in reactions catalyzed by aluminum bis(imino)pyridine compounds,[14] ruthenium tetraphosphine derivatives,[8f] and iron complexes bearing PNP pincer ligands.[7d, 7f] In contrast to *β*-hydride elimination, the hydride migration takes place in two-steps, on a saturated intermediate, which involve the slippage of the metal center from the coordinated oxygen into the free hydrogen and the subsequent CO_2 release. In order to discern between *β*-hydride elimination and hydride abstraction, DFT calculations (B3LYP(GD3)//6-31G**/SDD(f))

were carried out. The changes in $\Delta G^{\ddagger}$ were calculated in toluene at 298 K and 1 atmosphere. Although the reaction is slightly endergonic, the equilibrium is driven by removal of the gas.

Figure 9 summarizes the energy profile for the *β*-hydride elimination pathway. Because the formate complex **4** is saturated, the dissociation of the oxygen atom of the pincer is necessary in order to generate a coordination vacancy at the metal center, which allows the migration of the hydrogen atom of the formate group. The dissociation has an activation energy of 16.3 kcal·mol^{-1}, which is lower than the experimental values obtained for the activation energies of the catalysis and for the stoichiometric decarboxylation of **4**, and leads to a 16 e^{-} trihydride-hydroxo-osmium (IV) intermediate **C**. The latter is 13.9 kcal·mol^{-1} less stable than **4**. The migration leads to the Os (η^2-O=CO)-derivative **D**. Its barrier of 24.1 kcal·mol^{-1} with regard to **4** lies at the experimental upper limit. Intermediate **D** is 4.4 kcal·mol^{-1} less stable than **C**. The dissociation of the coordinated CO_2 molecule occurs in two steps, involving the sequential cleavage of the Os-C and Os-O bonds. Initially, intermediate **D** frees the carbon atom to afford **E**, which subsequently undergoes the Os-O rupture. The barrier for the first step of 26.8 kcal·mol^{-1}, with regard to **4**, is out of the experimental range and suggests that the *β*-hydride elimination is also a non-operating pathway. The release of the CO_2 molecule leads to **F**, which is a structural isomer of **5**.

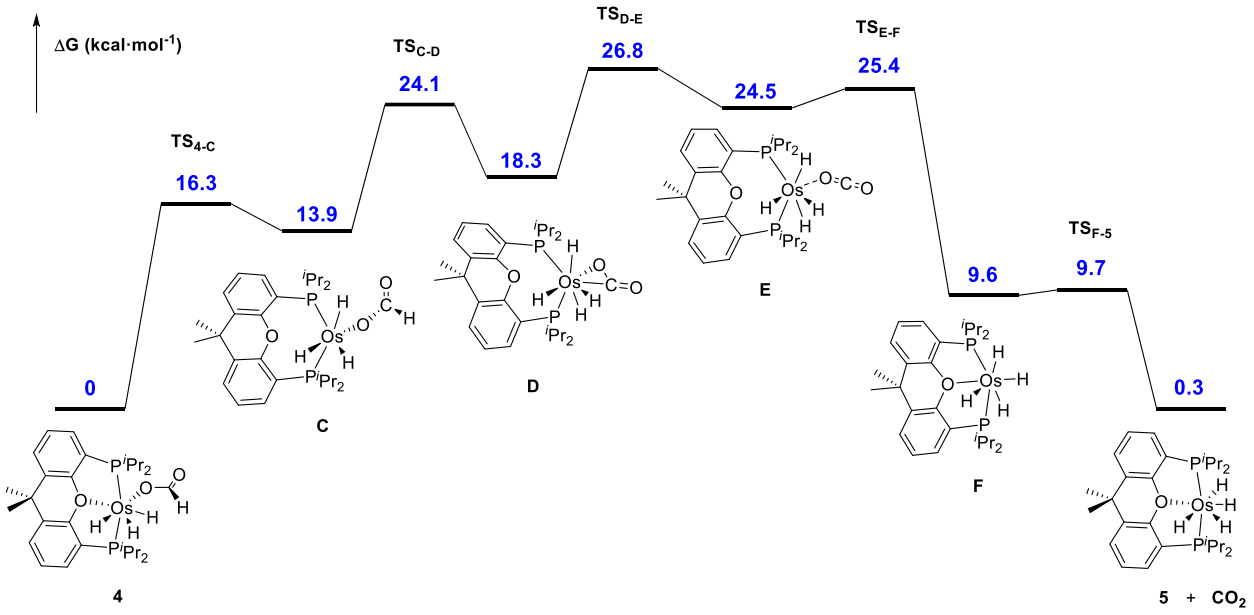

Figure 9. Energy profile (ΔG in kcal·mol^{-1}) for the CO_2 formation via β-hydride elimination.

The hydride abstraction takes place via intermediate **G** (Figure 10), which can be described as an Os{κ^1-H-(HCO_2)}-species and lies 12.1 kcal·mol^{-1} above **4**. Intermediate **G** is generated by means of the slippage of the metal center from the coordinated oxygen into the free hydrogen, following a formate O-C-H path. The process has an activation energy of 22.5 kcal·mol^{-1}, which compares well with the experimental values obtained for the catalysis and for the stoichiometric release of the CO_2 molecule from **4**. The agreement between the three values strongly supports a hydride abstraction mechanism for the CO_2 formation stage and reveals that the slippage of the metal center from the oxygen to the hydrogen through the formate O-C-H path is the rate determining step of the CO_2 formation stage and therefore of the catalysis. According to this, the release of CO_2 from **G** is a barrierless process.

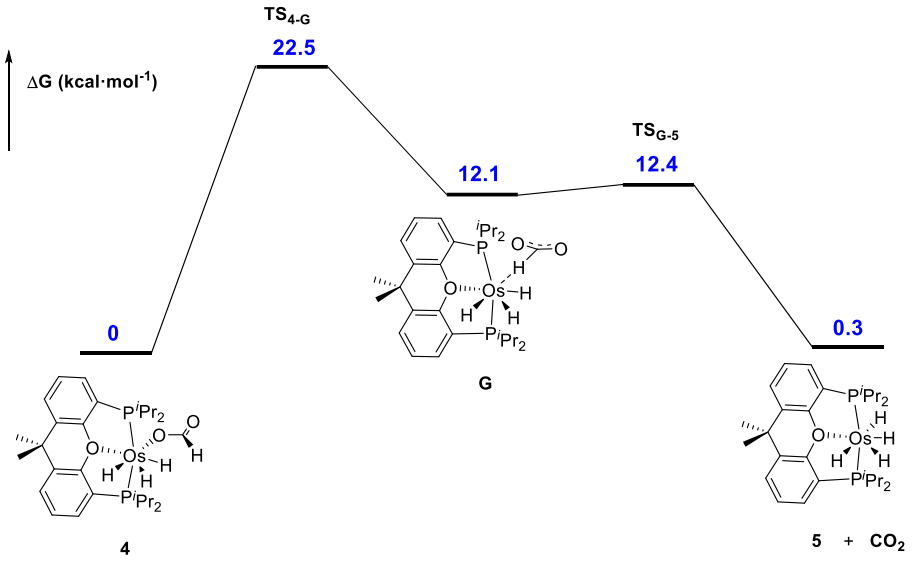

Figure 10. Energy profile (ΔG in kcal·mol^{-1}) for the CO_2 formation via hydride abstraction.

CONCLUDING REMARKS

Replacement of the chloride ligand of the trihydride $OsH_3Cl\{xant(P^iPr_2)_2\}$ by a hydroxo group affords the trihydride-hydroxo-osmium(IV) derivative $OsH_3(OH)\{xant(P^iPr_2)_2\}$ which efficiently promotes the FA dehydrogenation to CO_2 and H_2.

The dehydrogenation takes place through the catalytic cycle shown in Scheme 5. Under catalytic conditions the trihydride-hydroxo complex reacts with FA to form the compound $OsH_3\{\kappa^1\text{-}O\text{-}(HCO_2)\}\{xant(P^iPr_2)_2\}$, which has been isolated and fully characterized. DFT calculations suggest that the slippage of the metal center from the oxygen to the hydrogen through the formate O-C-H path affords an $OsH_3\{\kappa^1\text{-}H\text{-}(HCO_2)\}\{xant(P^iPr_2)_2\}$ intermediate, which releases CO_2 to give the previously described tetrahydride $OsH_4\{xant(P^iPr_2)_2\}$. The latter undergoes protonation with formic acid. According to previous DFT calculations, the resulting OsH_5-cation exists as an equilibrium mixture of two tautomers: the trihydride-compressed dihydride $[OsH_3(H\cdots H)\{xant(P^iPr_2)_2\}]^+$ and the hydride-compressed dihydride-dihydrogen

$[OsH(H\cdots H)(\eta^2\text{-}H_2)\{xant(P^iPr_2)_2\}]^+$. The dissociation of the coordinated H_2 molecule from the latter affords the unsaturated cation $[OsH_3\{xant(P^iPr_2)_2\}]^+$, which coordinates the formate anion to regenerate the trihydride-formate and to close the cycle. The slippage of the metal center from the oxygen to the hydrogen through the formate O-C-H path is the rate-determining step of the catalysis.

Scheme 5. Catalytic Cycle for the Formic Acid Dehydrogenation Promoted by 3

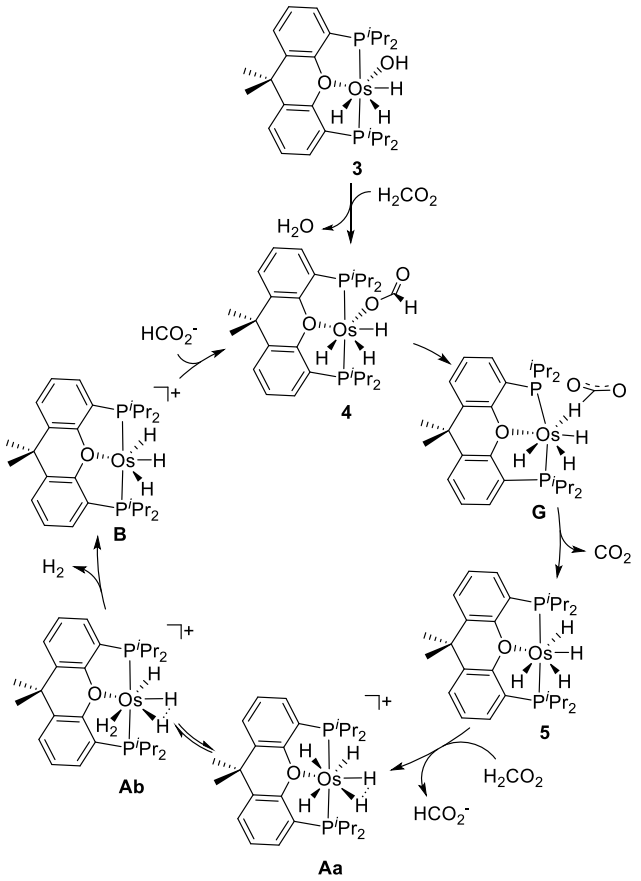

In conclusion, the first osmium catalyst for the FA dehydrogenation to CO_2 and H_2 has been discovered and the mechanism of the catalysis has been established, including the full characterization of the key intermediates and the elucidation of the rate-determining step.

EXPERIMENTAL SECTION

Preparation and characterization of complexes **2**, **3** and **4**, instrumental methods, NMR spectra, X-ray diffraction analysis information and DFT computational details are included in the Supporting Information.

General Methods for Formic Acid Dehydrogenation Studies. A solution of $OsH_3(OH)\{xant(P^iPr_2)_2\}$ (**3**) in 2.5 mL of toluene was syringed through a septum into a 25 mL flask immersed into a thermostatted bath, which was connected to a gas burette provided with a vaseline oil reservoir. Once the system had equilibrated to atmospheric pressure, formic acid was syringed and the solution was shaken (500 rpm). The reaction was followed by measuring the volume of the formed gas ($H_2 + CO_2$) with the time.

NMR Spectroscopic Studies of the Decarboxylation of $OsH_3\{\kappa^1\text{-}O\text{-}(HCO_2)\}\{xant(P^iPr_2)_2\}$ (4). The decarboxylation of complex **4** was followed by $^{31}P\{^1H\}$ NMR spectroscopy, in the temperature range T = 303 to 323 K. To a screw-top NMR tube containing a solution of $OsH_3(OH)\{xant(P^iPr_2)_2\}$ (**3**) (20.8 mg, 0.032 mmol) in toluene-d_8 (0.5 mL), and a capillary tube with a solution of PPh_3 in toluene-d_8 as internal standard, was added H_2CO_2 (1.2 μL, 0.032 mmol) via syringe. After 5 min, NMR spectra were recorded at the desired temperature, to show the formation of $OsH_4\{xant(P^iPr_2)_2\}$ (**5**) as a function of the time. The parameters of the $^{31}P\{^1H\}$ NMR experiment were modified to allow the integration of the signals: pulse program (zgig), $d_1 \geq 5T_1$ (d_1 = 20 s). The k_{st} value was obtained for each temperature from a plot Ln[**4**] / Ln[**4**]$_0$ vs time (eq 5).

ASSOCIATED CONTENT

Supporting Information

The Suporting Information is available free of charge.

Preparation and characterization of complexes **2**, **3** and **4**, instrumental methods, NMR spectra, X-ray diffraction analysis information and DFT computational details (PDF)

Cartesian coordinates of the calculated structures (XYZ)

AUTHOR INFORMATION

Corresponding Author

*E-mail for M.A.E.: maester@unizar.es.

ORCID

Miguel A. Esteruelas: 0000-0002-4829-7590

Cristina García-Yebra: 0000-0002-5545-5112

Jaime Martín: 0000-0003-0909-3509

Enrique Oñate: 0000-0003-2094-719X

Notes

The authors declare no competing financial interest.

ACKNOWLEDGMENT

We thank MINECO of Spain (Projects CTQ2017-82935-P and Red de Excelencia Consolider CTQ2016-81797-REDC), Diputación General de Aragón (E06_17R), FEDER, and the European Social Fund for financial support.

REFERENCES

(1) (a) Marbán, G.; Valdés-Solís, T. Towards the Hydrogen Economy? *Int. J. Hydrogen. Energ.* **2007**, *32*, 1625-1637. (b) Nikolaidis, P.; Poullikkas, A. A Comparative Overview of Hydrogen Production Processes. *Renew. Sust. Energ. Rev.* **2017**, *67*, 597-611.

(2) (a) Schlapbach, L.; Züttel, A. Hydrogen-Storage Materials for Mobile Applications. *Nature* **2001**, *414*, 353-358. (b) Yadav, M.; Xu, Q. Liquid-Phase Chemical Hydrogen Storage Materials. *Energy Environ. Sci.* **2012**, *5*, 9698-9725. (c) Dalebrook, A. F.; Gan, W. J.; Grasemann, M.; Moret, S.; Laurenczy, G. Hydrogen Storage: Beyond Conventional Methods. *Chem. Commun.* **2013**, *49*, 8735-8751. (d) Niaz, S.; Manzoor, T.; Pandith, A. H. Hydrogen Storage: Materials, Methods and Perspectives. *Renew. Sust. Energ. Rev.* **2015**, *50*, 457-469. (e) He, T.; Pachfule, P.; Wu, H.; Xu, Q.; Chen, P. Hydrogen Carriers. *Nat. Rev. Mater.* **2016**, *1*, 16059.

(3) Gianotti, E.; Taillades-Jacquin, M.; Rozière, J.; Jones, D. J. High-Purity Hydrogen Generation via Dehydrogenation of Organic Carriers: A Review on the Catalytic Process. *ACS Catal.* **2018**, *8*, 4660-4680.

(4) (a) Grasemann, M.; Laurenczy, G. Formic Acid as a Hydrogen Source – Recent Developments and Future Trends. *Energy Environ. Sci.* **2012**, *5*, 8171-8181. (b) Kawanami, H.; Himeda, Y.; Laurenczy, G. Formic Acid as a Hydrogen Carrier for Fuel Cells Toward a Sustainable Energy System. *Adv. Inorg. Chem.* **2017**, *70*, 395-427. (c) Eppinger, J.; Huang, K. W. Formic Acid as a Hydrogen Energy Carrier. *ACS Energy Lett.* **2017**, *2*, 188-195.

(5) (a) Filonenko, G. A.; van Putten, R.; Schulpen, E. N.; Hensen, E. J. M.; Pidko, E. A. Highly Efficient Reversible Hydrogenation of Carbon Dioxide to Formates Using a Ruthenium PNP-Pincer Catalyst. *ChemCatChem* **2014**, *6*, 1526-1530. (b) Wang, W. H.; Himeda, Y.; Muckerman, J. T.; Manbeck, G. F.; Fujita, E. CO_2 Hydrogenation to Formate and Methanol as an Alternative to Photo- and Electrochemical CO_2 Reduction. *Chem. Rev.* **2015**, *115*, 12936-12973. (c) Bernskoetter, W. H.; Hazari, N. Reversible Hydrogenation of Carbon Dioxide to Formic Acid and Methanol: Lewis Acid Enhancement of Base Metal Catalysts. *Acc. Chem. Res.* **2017**, *50*,

1049-1058. (d) Artz, J.; Müller, T. E.; Thenert, K.; Kleinekorte, J.; Meys, R.; Sternberg, A.; Bardow, A.; Leitner, W. Sustainable Conversion of Carbon Dioxide: An Integrated Review of Catalysis and Life Cycle Assessment. *Chem. Rev.* **2018**, *118*, 434-504.

(6) (a) Singh, A. K.; Singh, S.; Kumar, A. Hydrogen Energy Future with Formic Acid: a Renewable Chemical Hydrogen Storage System. *Catal. Sci. Technol.* **2016**, *6*, 12-40. (b) Mellmann, D.; Sponholz, P.; Junge, H.; Beller, M. Formic Acid as a Hydrogen Storage Material – Development of Homogeneous Catalysts for Selective Hydrogen Release. *Chem. Soc. Rev.* **2016**, *45*, 3954-3988. (c) Sordakis, K.; Tang, C. H.; Vogt, L. K.; Junge, H.; Dyson, P. J.; Beller, M.; Laurenczy, G. Homogeneous Catalysis for Sustainable Hydrogen Storage in Formic Acid and Alcohols. *Chem. Rev.* **2018**, *118*, 372-433. (d) Wang, X.; Meng, Q. L.; Gao, L. Q.; Jin, Z.; Ge, J. J.; Liu, C. P.; Xing, W. Recent Progress in Hydrogen Production from Formic Acid Decomposition. *Int. J. Hydrogen. Energ.* **2018**, *43*, 7055-7071.

(7) See for example: (a) Boddien, A.; Gärtner, F.; Jackstell, R.; Junge, H.; Spannenberg, A.; Baumann, W.; Ludwig, R.; Beller, M. *ortho*-Metalation of Iron(0) Tribenzylphosphine Complexes: Homogeneous Catalysts for the Generation of Hydrogen from Formic Acid. *Angew. Chem., Int. Ed.* **2010**, *49*, 8993-8996. (b) Boddien, A.; Loges, B.; Gärtner, F.; Torborg, C.; Fumino, K.; Junge, H.; Ludwig, R.; Beller, M. Iron-Catalyzed Hydrogen Production from Formic Acid. *J. Am. Chem. Soc.* **2010**, *132*, 8924-8934. (c) Boddien, A.; Mellmann, D.; Gärtner, F.; Jackstell, R.; Junge, H.; Dyson, P. J.; Laurenczy, G.; Ludwig, R.; Beller, M. Efficient Dehydrogenation of Formic Acid Using an Iron Catalyst. *Science* **2011**, *333*, 1733-1736. (d) Zell, T.; Butschke, B.; Ben-David, Y.; Milstein, D. Efficient Hydrogen Liberation from Formic Acid Catalyzed by a Well-Defined Iron Pincer Complex under Mild Conditions. *Chem. - Eur. J.* **2013**, *19*, 8068-8072. (e) Zell, T.; Milstein, D. Hydrogenation and Dehydrogenation Iron Pincer

Catalysts Capable of Metal Ligand Cooperation by Aromatization/Dearomatization. *Acc. Chem. Res.* **2015**, *48*, 1979-1994. (f) Mellone, I.; Gorgas, N.; Bertini, F.; Peruzzini, M.; Kirchner, K.; Gonsalvi, L. Selective Formic Acid Dehydrogenation Catalyzed by Fe-PNP Pincer Complexes Based on the 2,6-Diaminopyridine Scaffold. *Organometallics* **2016**, *35*, 3344-3349.

(8) See for example: (a) Gan, W. J.; Snelders, D. J. M.; Dyson, P. J.; Laurenczy, G. Ruthenium(II)-Catalyzed Hydrogen Generation from Formic Acid using Cationic, Ammoniomethyl-Substituted Triarylphosphine Ligands. *ChemCatChem* **2013**, *5*, 1126-1132. (b) Mellone, I.; Peruzzini, M.; Rosi, L.; Mellmann, D.; Junge, H.; Beller, M.; Gonsalvi, L. Formic Acid Dehydrogenation Catalysed by Ruthenium Complexes Bearing the Tripodal Ligands Triphos and NP_3. *Dalton Trans.* **2013**, *42*, 2495-2501. (c) Guerriero, A.; Bricout, H.; Sordakis, K.; Peruzzini, M.; Monflier, E.; Hapiot, F.; Laurenczy, G.; Gonsalvi, L. Hydrogen Production by Selective Dehydrogenation of HCOOH Catalyzed by Ru-Biaryl Sulfonated Phosphines in Aqueous Solution. *ACS Catal.* **2014**, *4*, 3002-3012. (d) Czaun, M.; Goeppert, A.; Kothandaraman, J.; May, R. B.; Haiges, R.; Prakash, G. K. S.; Olah, G. A. Formic Acid As a Hydrogen Storage Medium: Ruthenium-Catalyzed Generation of Hydrogen from Formic Acid in Emulsions. *ACS Catal.* **2014**, *4*, 311-320. (e) Pan, Y. P.; Pan, C. L.; Zhang, Y. F.; Li, H. F.; Min, S. X.; Guo, X. M.; Zheng, B.; Chen, H. L.; Anders, A.; Lai, Z. P.; Zheng, J. R.; Huang, K. W. Selective Hydrogen Generation from Formic Acid with Well-Defined Complexes of Ruthenium and Phosphorus-Nitrogen PN^3-Pincer Ligand. *Chem. - Asian J.* **2016**, *11*, 1357-1360. (f) Mellone, I.; Bertini, F.; Peruzzini, M.; Gonsalvi, L. An Active, Stable and Recyclable Ru(II) Tetraphosphine-Based Catalytic System for Hydrogen Production by Selective Formic Acid Dehydrogenation. *Catal. Sci. Technol.* **2016**, *6*, 6504-6512. (g) Anderson, N. H.; Boncella, J. M.; Tondreau, A. M. Reactivity of Silanes with (^{tBu}PONOP)Ruthenium Dichloride: Facile Synthesis

of Chloro-Silyl Ruthenium Compounds and Formic Acid Decomposition. *Chem. - Eur. J.* **2017**, *23*, 13617-13622. (h) Piola, L.; Fernández-Salas, J. A.; Nahra, F.; Poater, A.; Cavallo, L.; Nolan, S. P. Ruthenium-Catalysed Decomposition of Formic Acid: Fuel Cell and Catalytic Applications. *Mol. Catal.* **2017**, *440*, 184-189. (i) Guan, C.; Zhang, D. D.; Pan, Y. P.; Iguchi, M.; Ajitha, M. J.; Hu, J. S.; Li, H. F.; Yao, C. G.; Huang, M. H.; Ming, S. X.; Zheng, J. R.; Himeda, Y.; Kawanami, H.; Huang, K. W. Dehydrogenation of Formic Acid Catalyzed by a Ruthenium Complex with an *N,N'*-Diimine Ligand. *Inorg. Chem.* **2017**, *56*, 438-445.

(9) See for example: (a) Celaje, J. J. A.; Lu, Z. Y.; Kedzie, E. A.; Terrile, N. J.; Lo, J. N.; Williams, T. J. A Prolific Catalyst for Dehydrogenation of Neat Formic Acid. *Nat. Commun.* **2016**, *7*, 11308. (b) Papp, G.; Ölveti, G.; Horváth, H.; Kathó, A.; Joó, F. Highly Efficient Dehydrogenation of Formic Acid in Aqueous Solution Catalysed by an Easily Available Water-Soluble Iridium(III) Dihydride. *Dalton Trans.* **2016**, *45*, 14516-14519. (c) Iguchi, M.; Himeda, Y.; Manaka, Y.; Kawanami, H. Development of an Iridium-Based Catalyst for High-Pressure Evolution of Hydrogen from Formic Acid. *ChemSusChem* **2016**, *9*, 2749-2753. (d) Li, J. J.; Li, J. H.; Zhang, D. J.; Liu, C. B. DFT Study on the Mechanism of Formic Acid Decomposition by a Well-Defined Bifunctional Cyclometalated Iridium(III) Catalyst: Self-Assisted Concerted Dehydrogenation via Long-Range Intermolecular Hydrogen Migration. *ACS Catal.* **2016**, *6*, 4746-4754. (e) Czaun, M.; Kothandaraman, J.; Goeppert, A.; Yang, B.; Greenberg, S.; May, R. B.; Olah, G. A.; Prakash, G. K. S. Iridium-Catalyzed Continuous Hydrogen Generation from Formic Acid and Its Subsequent Utilization in a Fuel Cell: Toward a Carbon Neutral Chemical Energy Storage. *ACS Catal.* **2016**, *6*, 7475-7484. (f) Iguchi, M.; Zhong, H.; Himeda, Y.; Kawanami, H. Kinetic Studies on Formic Acid Dehydrogenation Catalyzed by an Iridium Complex towards Insights into the Catalytic Mechanism of High-Pressure Hydrogen Gas

Production. *Chem. - Eur. J.* **2017**, *23*, 17017-17021. (g) Wang, L.; Onishi, N.; Murata, K.; Hirose, T.; Muckerman, J. T.; Fujita, E.; Himeda, Y. Efficient Hydrogen Storage and Production Using a Catalyst with an Imidazoline-Based, Proton-Responsive Ligand. *ChemSusChem* **2017**, *10*, 1071-1075. (h) Cohen, S.; Borin, V.; Schapiro, I.; Musa, S.; De-Botton, S.; Belkova, N. V.; Gelman, D. Ir(III)-PC(sp^3)P Bifunctional Catalysts for Production of H_2 by Dehydrogenation of Formic Acid: Experimental and Theoretical Study. *ACS Catal.* **2017**, *7*, 8139-8146. (i) Iguchi, M.; Zhong, H.; Himeda, Y.; Kawanami, H. Effect of the *ortho*-Hydroxyl Groups on a Bipyridine Ligand of Iridium Complexes for the High-Pressure Gas Generation from the Catalytic Decomposition of Formic Acid. *Chem. - Eur. J.* **2017**, *23*, 17788-17793. (j) Lu, S. M.; Wang, Z. J.; Wang, J. J.; Li, J.; Li, C. Hydrogen Generation from Formic Acid Decomposition on a Highly Efficient Iridium Catalyst Bearing a Diaminoglyoxime Ligand. *Green Chem.* **2018**, *20*, 1835-1840.

(10) Neary, M. C.; Parkin, G. Dehydrogenation, Disproportionation and Transfer Hydrogenation Reactions of Formic Acid Catalyzed by Molybdenum Hydride Compounds. *Chem. Sci.* **2015**, *6*, 1859-1865.

(11) Fink, C.; Laurenczy, G. CO_2 as a Hydrogen Vector – Transition Metal Diamine Catalysts for Selective HCOOH Dehydrogenation. *Dalton Trans.* **2017**, *46*, 1670-1676.

(12) Enthaler, S.; Brück, A.; Kammer, A.; Junge, H.; Irran, E.; Gülak, S. Exploring the Reactivity of Nickel Pincer Complexes in the Decomposition of Formic Acid to CO_2/H_2 and the Hydrogenation of $NaHCO_3$ to HCOONa. *ChemCatChem* **2015**, *7*, 65-69.

(13) Correa, A.; Cascella, M.; Scotti, N.; Zaccheria, F.; Ravasio, N.; Psaro, R. Mechanistic Insights into Formic Acid Dehydrogenation Promoted by Cu-Amino Based Systems. *Inorg. Chim. Acta.* **2018**, *470*, 290-294.

(14) Myers, T. W.; Berben, L. A. Aluminium-Ligand Cooperation Promotes Selective Dehydrogenation of Formic Acid to H_2 and CO_2. *Chem. Sci.* **2014**, *5*, 2771-2777.

(15) Iglesias, M.; Oro, L. A. Mechanistic Considerations on Homogeneously Catalyzed Formic Acid Dehydrogenation. *Eur. J. Inorg. Chem.* **2018**, 2125-2138.

(16) (a) Dub, P. A.; Henson, N. J.; Martin, R. L.; Gordon, J. C. Unravelling the Mechanism of the Asymmetric Hydrogenation of Acetophenone by [RuX_2(diphosphine)(1,2-diamine)] Catalysts. *J. Am. Chem. Soc.* **2014**, *136*, 3505-3521. (b) Dub, P. A.; Gordon, J. C. The Mechanism of Enantioselective Ketone Reduction with Noyori and Noyori-Ikariya Bifunctional Catalysts. *Dalton Trans.* **2016**, *45*, 6756-6781. (c) Gusev, D. G. Dehydrogenative Coupling of Ethanol and Ester Hydrogenation Catalyzed by Pincer-Type YNP Complexes. *ACS Catal.* **2016**, *6*, 6967-6981. (d) Morris, S. A.; Gusev, D. G. Rethinking the Claisen-Tishchenko Reaction. *Angew. Chem., Int. Ed.* **2017**, *56*, 6228-6231. (e) Dub, P. A.; Gordon, J. C. Metal Ligand Bifunctional Catalysis: The "Accepted" Mechanism, the Issue of Concertedness, and the Function of the Ligand in Catalytic Cycles Involving Hydrogen Atoms. *ACS Catal.* **2017**, *7*, 6635-6655. (f) Gusev, D. G. Rethinking the Dehydrogenative Amide Synthesis. *ACS Catal.* **2017**, *7*, 6656-6662.

(17) (a) Kolb, H. C.; VanNieuwenhze, M. S.; Sharpless, K. B. Catalytic Asymmetric Dihydroxylation. *Chem. Rev.* **1994**, *94*, 2483-2547. (b) Döbler, C.; Mehltretter, G. M.; Sundermeier, U.; Beller, M. Osmium-Catalyzed Dihydroxylation of Olefins Using Dioxygen or

Air as the Terminal Oxidant. *J. Am. Chem. Soc.* **2000**, *122*, 10289-10297. (c) Döbler, C.; Mehltretter, G. M.; Sundermeier, U.; Beller, M. Dihydroxylation of Olefins Using Air as the Terminal Oxidant. *J. Organomet. Chem.* **2001**, *621*, 70-76. (d) Heravi, M. M.; Zadsirjan, V.; Esfandyari, M.; Lashaki, T. B. Applications of Sharpless Asymmetric Dihydroxylation in the Total Synthesis of Natural Products. *Tetrahedron: Asymmetry* **2017**, *28*, 987-1043.

(18) See for example: (a) Sánchez-Delgado, R. A.; Rosales, M.; Esteruelas, M. A.; Oro, L. A. Homogeneous Catalysis by Osmium Complexes - a Review. *J. Mol. Catal. A: Chem.* **1995**, *96*, 231-243. (b) Esteruelas, M. A.; Herrero, J.; López, A. M.; Oliván, M. Alkyne-Coupling Reactions Catalyzed by $OsHCl(CO)(P^iPr_3)_2$ in the Presence of Diethylamine. *Organometallics* **2001**, *20*, 3202-3205. (c) Castarlenas, R.; Esteruelas, M. A.; Oñate, E. N-Heterocyclic Carbene-Osmium Complexes for Olefin Metathesis Reactions. *Organometallics* **2005**, *24*, 4343-4346. (d) Esteruelas, M. A.; García-Yebra, C.; Oliván, M.; Oñate, E.; Valencia, M. Osmium-Catalyzed Allylic Alkylation. *Organometallics* **2008**, *27*, 4892-4902. (e) Batuecas, M.; Esteruelas, M. A.; García-Yebra, C.; Oñate, E. Redox Isomerization of Allylic Alcohols Catalyzed by Osmium and Ruthenium Complexes Containing a Cyclopentadienyl Ligand with a Pendant Amine or Phosphoramidite Group: X-ray Structure of an η^3-1-Hydroxyallyl-Metal-Hydride Intermediate. *Organometallics* **2010**, *29*, 2166-2175. (f) Varela-Fernández, A.; García-Yebra, C.; Varela, J. A.; Esteruelas, M. A.; Saá, C. Osmium-Catalyzed 7-*endo* Heterocyclization of Aromatic Alkynols into Benzoxepines. *Angew. Chem., Int. Ed.* **2010**, *49*, 4278-4281. (g) Wu, L. P.; Liu, Q.; Spannenberg, A.; Jackstell, R.; Beller, M. Highly Regioselective Osmium-Catalyzed Hydroformylation. *Chem. Commun.* **2015**, *51*, 3080-3082. (h) Álvarez-Pérez, A.; González-Rodríguez, C.; García-Yebra, C.; Varela, J. A.; Oñate, E.; Esteruelas, M. A.; Saá, C. Catalytic Cyclization of *o*-Alkynyl Phenethylamines via Osmacyclopropene Intermediates: Direct Access

to Dopaminergic 3-Benzazepines. *Angew. Chem., Int. Ed.* **2015**, *54*, 13357-13361. (i) Batuecas, M.; Castro-Rodrigo, R.; Esteruelas, M. A.; García-Yebra, C.; López, A. M.; Oñate, E. Aromatic Osmacyclopropenefuran Bicycles and Their Relevance for the Metal-Mediated Hydration of Functionalized Allenes. *Angew. Chem., Int. Ed.* **2016**, *55*, 13749-13753. (j) González-Fernández, R.; Crochet, P.; Cadierno, V.; Menéndez, M. I.; López, R. Phosphinous Acid-Assisted Hydration of Nitriles: Understanding the Controversial Reactivity of Osmium and Ruthenium Catalysts. *Chem. - Eur. J.* **2017**, *23*, 15210-15221.

(19) See for example: (a) Esteruelas, M. A.; Oro, L. A.; Valero, C. Hydrogenation of Benzylideneacetone Catalyzed by $OsHCl(CO)(PR_3)_2$ (PR_3 = P^iPr_3, PMe-^{t}Bu$_2$) - New Roles of Dihydrogen Complexes in Homogeneous Catalytic-Hydrogenation. *Organometallics* **1992**, *11*, 3362-3369. (b) Barrio, P.; Esteruelas, M. A.; Oñate, E. Reactions of a Hexahydride-Osmium Complex with Aldehydes: Double C-H_α Activation-Decarbonylation and Single C-H_α Activation-Hydroxylation Tandem Processes and Catalytic Tishchenko Reactions. *Organometallics* **2004**, *23*, 1340-1348. (c) Esteruelas, M. A.; Honczek, N.; Oliván, M.; Oñate, E.; Valencia, M. Direct Access to POP-Type Osmium(II) and Osmium(IV) Complexes: Osmium a Promising Alternative to Ruthenium for the Synthesis of Imines from Alcohols and Amines. *Organometallics* **2011**, *30*, 2468-2471. (d) Baratta, W.; Bossi, G.; Putignano, E.; Rigo, P. Pincer and Diamine Ru and Os Diphosphane Complexes as Efficient Catalysts for the Dehydrogenation of Alcohols to Ketones. *Chem. - Eur. J.* **2011**, *17*, 3474-3481. (e) Bertoli, M.; Choualeb, A.; Lough, A. J.; Moore, B.; Spasyuk, D.; Gusev, D. G. Osmium and Ruthenium Catalysts for Dehydrogenation of Alcohols. *Organometallics* **2011**, *30*, 3479-3482. (f) Spasyuk, D.; Gusev, D. G. Acceptorless Dehydrogenative Coupling of Ethanol and Hydrogenation of Esters and Imines. *Organometallics* **2012**, *31*, 5239-5242. (g) Spasyuk, D.; Vicent, C.; Gusev, D. G.

Chemoselective Hydrogenation of Carbonyl Compounds and Acceptorless Dehydrogenative Coupling of Alcohols. *J. Am. Chem. Soc.* **2015**, *137*, 3743-3746. (h) Chelucci, G.; Baldino, S.; Baratta, W. Ruthenium and Osmium Complexes Containing 2-(aminomethyl)pyridine (Ampy)-Based Ligands in Catalysis. *Coord. Chem. Rev.* **2015**, *300*, 29-85. (i) Chelucci, G.; Baldino, S.; Baratta, W. Recent Advances in Osmium-Catalyzed Hydrogenation and Dehydrogenation Reactions. *Acc. Chem. Res.* **2015**, *48*, 363-379. (j) Bolaño, T.; Esteruelas, M. A.; Gay, M. P.; Oñate, E.; Pastor, I. M.; Yus, M. An Acyl-NHC Osmium Cooperative System: Coordination of Small Molecules and Heterolytic B-H and O-H Bond Activation. *Organometallics* **2015**, *34*, 3902-3908. (k) Chelucci, G. Ruthenium and Osmium Complexes in C-C Bond-Forming Reactions by Borrowing Hydrogen Catalysis. *Coord. Chem. Rev.* **2017**, *331*, 1-36.

(20) Esteruelas, M. A.; López, A. M.; Oliván, M. Polyhydrides of Platinum Group Metals: Nonclassical Interactions and σ-Bond Activation Reactions. *Chem. Rev.* **2016**, *116*, 8770-8847.

(21) (a) Esteruelas, M. A.; Fernández, I.; López, A. M.; Mora, M.; Oñate, E. Osmium-Promoted Dehydrogenation of Amine-Boranes and B-H Bond Activation of the Resulting Amino-Boranes. *Organometallics* **2014**, *33*, 1104-1107. (b) Esteruelas, M. A.; López, A. M.; Mora, M.; Oñate, E. Ammonia-Borane Dehydrogenation Promoted by an Osmium Dihydride Complex: Kinetics and Mechanism. *ACS Catal.* **2015**, *5*, 187-191.

(22) (a) Esteruelas, M. A.; Lezáun, V.; Martínez, A.; Oliván, M.; Oñate, E. Osmium Hydride Acetylacetonate Complexes and Their Application in Acceptorless Dehydrogenative Coupling of Alcohols and Amines and for the Dehydrogenation of Cyclic Amines. *Organometallics* **2017**, *36*, 2996-3004. (b) Buil, M. L.; Esteruelas, M. A.; Gay, M. P.; Gómez-Gallego, M.; Nicasio, A. I.; Oñate, E.; Santiago, A.; Sierra, M. A. Osmium Catalysts for Acceptorless and Base-Free

Dehydrogenation of Alcohols and Amines: Unusual Coordination Modes of a BPI Anion. *Organometallics* **2018**, *37*, 603-617.

(23) Castarlenas, R.; Esteruelas, M. A.; Oñate, E. Preparation, X-ray Structure, and Reactivity of an Osmium-Hydroxo Complex Stabilized by an N-Heterocyclic Carbene Ligand: A Base-Free Catalytic Precursor for Hydrogen Transfer from 2-Propanol to Aldehydes. *Organometallics* **2008**, *27*, 3240-3247.

(24) Buil, M. L.; Esteruelas, M. A.; Herrero, J.; Izquierdo, S.; Pastor, I. M.; Yus, M. Osmium Catalyst for the Borrowing Hydrogen Methodology: *α*-Alkylation of Arylacetonitriles and Methyl Ketones. *ACS Catal.* **2013**, *3*, 2072-2075.

(25) Buil, M. L.; Cadierno, V.; Esteruelas, M. A.; Gimeno, J.; Herrero, J.; Izquierdo, S.; Oñate, E. Selective Hydration of Nitriles to Amides Promoted by an Os-NHC Catalyst: Formation and X-ray Characterization of κ^2-Amidate Intermediates. *Organometallics* **2012**, *31*, 6861-6867.

(26) Nelson, D. J.; Nolan, S. P. Hydroxide Complexes of the Late Transition Metals: Organometallic Chemistry and Catalysis. *Coord. Chem. Rev.* **2017**, *353*, 278-294.

(27) Ozerov, O. V. Oxidative Addition of Water to Transition Metal Complexes. *Chem. Soc. Rev.* **2009**, *38*, 83-88.

(28) (a) Gotzig, J.; Werner, R.; Werner, H. Basic Metals: 53. Ruthenium- and Osmium-Complexes with Dimethylphosphinomethanide-Anion as Ligands. *J. Organomet. Chem.* **1985**, *290*, 99-114. (b) Edwards, A. J.; Elipe, S.; Esteruelas, M. A.; Lahoz, F. J.; Oro, L. A.; Valero, C. Synthesis and Reactivity of the Unusual Five-Coordinate Hydrido-Hydroxo Complex $OsH(OH)(CO)(P^iPr_3)_2$. *Organometallics* **1997**, *16*, 3828-3836. (c) Renkema, K. B.; Huffman, J.

C.; Caulton, K. G. Characterization and Structure of $OsH(OH)(CO)(PBu_2Me)^tBu_2$. *Polyhedron* **1999**, *18*, 2575-2578. (d) Prokopchuk, D. E.; Collado, A.; Lough, A. J.; Morris, R. H. Structural Properties of *trans* Hydrido-Hydroxo $M(H)(OH)(NH_2CMe_2CMe_2NH_2)(PPh_3)_2$ (M = Ru, Os) Complexes and their Proton Exchange Behaviour with Water in Solution. *Dalton Trans.* **2013**, *42*, 10214-10220. (e) Buil, M. L.; Cardo, J. J. F.; Esteruelas, M. A.; Fernández, I.; Oñate, E. Hydroboration and Hydrogenation of an Osmium-Carbon Triple Bond: Osmium Chemistry of a Bis-*σ*-Borane. *Organometallics* **2015**, *34*, 547-550.

(29) *Pincer Compounds: Chemistry and Applications*; Ed.: Morales-Morales, D. Elsevier, 2018.

(30) (a) Pontiggia, A. J.; Chaplin, A. B.; Weller, A. S. Cationic Iridium Complexes of the Xantphos Ligand. Flexible Coordination Modes and the Isolation of the Hydride Insertion Product with an Alkene. *J. Organomet. Chem.* **2011**, *696*, 2870-2876. (b) Dallanegra, R.; Chaplin, A. B.; Weller, A. S. Rhodium Cyclopentyl Phosphine Complexes of Wide-Bite-Angle Ligands DPEphos and Xantphos. *Organometallics* **2012**, *31*, 2720-2728. (c) Alós, J.; Bolaño, T.; Esteruelas, M. A.; Oliván, M.; Oñate, E.; Valencia, M. POP-Pincer Osmium-Polyhydrides: Head-to-Head (*Z*)-Dimerization of Terminal Alkynes. *Inorg. Chem.* **2013**, *52*, 6199-6213. (d) Johnson, H. C.; Torry-Harris, R.; Ortega, L.; Theron, R.; McIndoe, J. S.; Weller, A. S. Exploring the Mechanism of the Hydroboration of Alkenes by Amine-Boranes Catalysed by $[Rh(xantphos)]^+$. *Catal. Sci. Technol.* **2014**, *4*, 3486-3494. (e) Johnson, H. C.; Leitao, E. M.; Whitten, G. R.; Manners, I.; Lloyd-Jones, G. C.; Weller, A. S. Mechanistic Studies of the Dehydrocoupling and Dehydropolymerization of Amine-Boranes Using a $[Rh(Xantphos)]^+$ Catalyst. *J. Am. Chem. Soc.* **2014**, *136*, 9078-9093. (f) Johnson, H. C.; Weller, A. S. P-C-Activated Bimetallic Rhodium Xantphos Complexes: Formation and Catalytic Dehydrocoupling of Amine-Boranes. *Angew. Chem., Int. Ed.* **2015**, *54*, 10173-10177. (g) Ren, P.; Pike, S. D.;

Pernik, I.; Weller, A. S.; Willis, M. C. Rh-POP Pincer Xantphos Complexes for C-S and C-H Activation. Implications for Carbothiolation Catalysis. *Organometallics* **2015**, *34*, 711-723. (h) Esteruelas, M. A.; Nolis, P.; Oliván, M.; Oñate, E.; Vallribera, A.; Vélez, A. Ammonia Borane Dehydrogenation Promoted by a Pincer-Square-Planar Rhodium(I) Monohydride: A Stepwise Hydrogen Transfer from the Substrate to the Catalyst. *Inorg. Chem.* **2016**, *55*, 7176-7181. (i) Esteruelas, M. A.; García-Yebra, C.; Martín, J.; Oñate, E. *mer*, *fac*, and Bidentate Coordination of an Alkyl-POP Ligand in the Chemistry of Nonclassical Osmium Hydrides. *Inorg. Chem.* **2017**, *56*, 676-683. (j) Adams, G. M.; Weller, A. S. POP-type ligands: Variable Coordination and Hemilabile Behaviour. *Coord. Chem. Rev.* **2018**, *355*, 150-172. (k) Adams, G. M.; Colebatch, A. L.; Skornia, J. T.; McKay, A. I.; Johnson, H. C.; Lloyd-Jones, G. C.; Macgregor, S. A.; Beattie, N. A.; Weller, A. S. Dehydropolymerization of $H_3B{\cdot}NMeH_2$ To Form Polyaminoboranes Using [Rh(Xantphos-alkyl)] Catalysts. *J. Am. Chem. Soc.* **2018**, *140*, 1481-1495.

(31) (a) Asensio, G.; Cuenca, A. B.; Esteruelas, M. A.; Medio-Simón, M.; Oliván, M.; Valencia, M. Osmium(III) Complexes with POP Pincer Ligands: Preparation from Commercially Available $OsCl_3{\cdot}3H_2O$ and Their X-ray Structures. *Inorg. Chem.* **2010**, *49*, 8665-8667. (b) Alós, J.; Bolaño, T.; Esteruelas, M. A.; Oliván, M.; Oñate, E.; Valencia, M. POP-Pincer Ruthenium Complexes: d^6 Counterparts of Osmium d^4 Species. *Inorg. Chem.* **2014**, *53*, 1195-1209. (c) Alós, J.; Esteruelas, M. A.; Oliván, M.; Oñate, E.; Puylaert, P. C-H Bond Activation Reactions in Ketones and Aldehydes Promoted by POP-Pincer Osmium and Ruthenium Complexes. *Organometallics* **2015**, *34*, 4908-4921. (d) Esteruelas, M. A.; Fenández, I.; García-Yebra, C.; Martín, J.; Oñate, E. Elongated σ-Borane versus σ-Borane in Pincer-POP-Osmium Complexes. *Organometallics* **2017**, *36*, 2298-2307. (e) Esteruelas, M. A.; Oliván, M. Osmium Complexes with POP Pincer Ligands. In *Pincer Compounds*; 1st ed.; Morales-Morales, D.; Elsevier: 2018.

(32) (a) Esteruelas, M. A.; Oliván, M.; Vélez, A. Xantphos-Type Complexes of Group 9: Rhodium versus Iridium. *Inorg. Chem.* **2013**, *52*, 5339-5349. (b) Esteruelas, M. A.; Oliván, M.; Vélez, A. POP-Pincer Silyl Complexes of Group 9: Rhodium versus Iridium. *Inorg. Chem.* **2013**, *52*, 12108-12119. (c) Esteruelas, M. A.; Oliván, M.; Vélez, A. POP-Rhodium-Promoted C-H and B-H Bond Activation and C-B Bond Formation. *Organometallics* **2015**, *34*, 1911-1924. (d) Esteruelas, M. A.; Oliván, M.; Vélez, A. Conclusive Evidence on the Mechanism of the Rhodium-Mediated Decyanative Borylation. *J. Am. Chem. Soc.* **2015**, *137*, 12321-12329. (e) Curto, S. G.; Esteruelas, M. A.; Oliván, M.; Oñate, E.; Vélez, A. Selective C-Cl Bond Oxidative Addition of Chloroarenes to a POP-Rhodium Complex. *Organometallics* **2017**, *36*, 114-128.

(33) Wu, A.; Dehestani, A.; Saganic, E.; Crevier, T. J.; Kaminsky, W.; Cohen, D. E.; Mayer, J. M. Reactions of Tp-Os Nitrido Complexes with the Nucleophiles Hydroxide and Thiosulfate. *Inorg. Chim. Acta.* **2006**, *359*, 2842-2849.

(34) Kiefer, A. M.; Giles, J. A.; Shapley, P. A. Synthesis, Structure, and Reactivity of Organometallic Osmium(VI) Hydroxo Compounds. *Organometallics* **2007**, *26*, 1881-1887.

(35) (a) Gould, R. O.; Jones, C. L.; Stephenson, T. A.; Tocher, D. A. Structural Characterization of Hydroxo-Bridged Arene-Ruthenium and Arene-Osmium Complexes - Further Reactions of Hydroxo-Bridged Complexes. *J. Organomet. Chem.* **1984**, *264*, 365-378. (b) Cabeza, J. A.; Mann, B. E.; Maitlis, P. M.; Brevard, C. The Synthesis of Di-Nuclear and Tetra-Nuclear *p*-Cymene-Osmium Hydride Complexes - Characterization by ^{1}H (^{187}Os) Reverse INEPT Two-Dimensional Nuclear Magnetic-Resonance Spectroscopy. *J. Chem. Soc., Dalton Trans.* **1988**, 629-634. (c) Esteruelas, M. A.; García-Yebra, C.; Oliván, M.; Oñate, E. Reaction of a Cationic Osmium(IV) Dihydride with Ethylene: Formation and Structure of the Novel Tetraethylene

Dimer Complex [{(P^iPr_3)(η^2-C_2H_4)$_2$Os}$_2$(μ-OH)$_2$(μ-O_2CCH_3)]BF_4. *Organometallics* **2000**, *19*, 3260-3262. (d) Peacock, A. F. A.; Habtemariam, A.; Fernández, R.; Walland, V.; Fabbiani, F. P. A.; Parsons, S.; Aird, R. E.; Jodrell, D. I.; Sadler, P. J. Tuning the Reactivity of Osmium(II) and Ruthenium(II) Arene Complexes Under Physiological Conditions. *J. Am. Chem. Soc.* **2006**, *128*, 1739-1748.

(36) CO is not formed. In this context, it should be mentioned that both **3** and **5** react with this gas to afford $Os(CO)_3${κ^2-P,P-[xant(P^iPr_2)$_2$]} which is not active.

(37) See for example: (a) Scholten, J. D.; Prechtl, M. H. G.; Dupont, J. Decomposition of Formic Acid Catalyzed by a Phosphine-Free Ruthenium Complex in a Task-Specific Ionic Liquid. *ChemCatChem* **2010**, *2*, 1265-1270. (b) Wang, W. H.; Xu, S.; Manaka, Y.; Suna, Y.; Kambayashi, H.; Muckerman, J. T.; Fujita, E.; Himeda, Y. Formic Acid Dehydrogenation with Bioinspired Iridium Complexes: A Kinetic Isotope Effect Study and Mechanistic Insight. *ChemSusChem* **2014**, *7*, 1976-1983. (c) Wang, W. H.; Ertem, M. Z.; Xu, S. A.; Onishi, N.; Manaka, Y.; Suna, Y.; Kambayash, H.; Muckerman, J. T.; Fujita, E.; Himeda, Y. Highly Robust Hydrogen Generation by Bioinspired Ir Complexes for Dehydrogenation of Formic Acid in Water: Experimental and Theoretical Mechanistic Investigations at Different pH. *ACS Catal.* **2015**, *5*, 5496-5504. (d) Ertem, M. Z.; Himeda, Y.; Fujita, E.; Muckerman, J. T. Interconversion of Formic Acid and Carbon Dioxide by Proton-Responsive, Half-Sandwich Cp*Ir-III Complexes: A Computational Mechanistic Investigation. *ACS Catal.* **2016**, *6*, 600-609.

SYNOPSIS

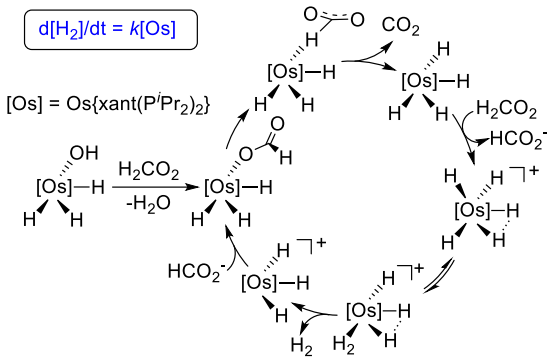
d[H2]/dt = k[Os]
[Os] = Os{xant(PiPr2)2}
[Os]—H
H2CO2
-H2O
CO2
H2CO2
HCO2-
HCO2-
H2